Research Square

Preprints are preliminary reports that have not undergone peer review.
They should not be considered conclusive, used to inform clinical practice,
or referenced by the media as validated information.

MRI-Based Normative Orbital Anthropometric Measurements in Pediatric Populations: Age-Related Variations and Clinical Implications

Cafer Ikbal Gulsever

cafer.gulsever@gmail.com

Hakkari State Hospital

Alaaddin Ates

Hakkari State Hospital

Elif Hazal Karlı

Istanbul University

Edanur Karapinar

Istanbul University

Zuhal Bayramoglu

Istanbul University

Mehmet Semih Cakir

Istanbul University

Gorkem Durak

Istanbul University

Serra Sencer

Istanbul University

Mehmet Barburoglu

Istanbul University

Research Article

Keywords:

Posted Date: September 15th, 2025

DOI: https://doi.org/10.21203/rs.3.rs-7224495/v1

License: This work is licensed under a Creative Commons Attribution 4.0 International License.
Read Full License

Additional Declarations: No competing interests reported.

Abstract

Purpose: Precise and reliable anthropometric reference data for the pediatric orbit is crucial for accurately diagnosing orbital disorders, detecting developmental abnormalities, and planning effective surgical interventions. This study aimed to establish comprehensive MRI-based normative orbital measurements in a pediatric population, explore clinically meaningful age-related variations, and assess measurement reliability across multiple neuroradiologists.

Methods: In this retrospective study, we analyzed MRI scans from 64 healthy pediatric patients (32 males, 32 females; age range 1–17 years) acquired at both 1.5 Tesla and 3 Tesla MRI systems. Patients were categorized into preschool (1–6 years), school-age (7–12 years), and adolescent (13–17 years) groups. Three expert neuroradiologists independently measured clinically relevant orbital parameters including extraocular muscle thicknesses, orbital breadth and height, interzygomatic distance, intercanthal distance, optic nerve sheath width, and optic nerve angle. Data were statistically evaluated using Spearman's correlation, Kruskal–Wallis tests, Mann–Whitney U tests, and intraclass correlation coefficients (ICCs) for reliability assessment.

Results: We provide detailed, MRI-derived normative data for essential pediatric orbital structures, highlighting significant and clinically meaningful age-dependent anatomical changes. Notably, the interzygomatic distance demonstrated the strongest correlation with age ($r=0.772$, $p<0.001$), underscoring its clinical relevance in developmental assessment. Orbital breadth (right: $r=0.674$; left: $r=0.703$) and orbital height (right: $r=0.608$; left: $r=0.644$; all $p<0.001$) also increased significantly with advancing age, offering clear reference values for clinical practice. Conversely, certain parameters such as optic nerve angle exhibited remarkable stability across age groups, providing consistent normative benchmarks. Interobserver reliability among neuroradiologists was excellent (orbital breadth ICC=0.92; orbital height ICC=0.90), reinforcing measurement robustness.

Conclusions: This study delivers precise MRI-based normative pediatric orbital anthropometric data, clearly identifying age-related developmental trends and stable anatomical landmarks. These reference measurements can significantly aid radiologists and surgeons in the accurate identification of orbital pathologies, the detection of subtle developmental anomalies, and in optimizing surgical planning and clinical outcomes in pediatric orbital cases.

Introduction

The orbit is an intricate anatomical region that houses the globe and provides structural attachments for the extraocular muscles, vasculature, and cranial nerves, which are critical for visual function and ocular motility [1]. A precise understanding of normative orbital anthropometric measurements is indispensable in clinical settings for accurately diagnosing and managing various pathologies, including orbital fractures, congenital craniofacial syndromes, endocrine ophthalmopathy, such as thyroid orbitopathy, inflammatory orbital conditions, and orbital tumors. Such measurements are essential for surgical planning, prosthetic reconstruction, and evaluating treatment outcomes [2, 3].

Historically, anthropometric evaluations of orbital structures have been predominantly conducted using CT, which leverages its high spatial resolution and accurate bone delineation [4, 5]. However, CT carries inherent risks associated with ionizing radiation exposure, particularly significant in pediatric populations due to increased vulnerability to radiation-induced carcinogenesis [6–8]. Conversely, MRI offers an optimal alternative, eliminating radiation exposure and providing superior delineation of soft tissues and neurovascular structures within the orbit [9].

Despite MRI's clear advantages, comprehensive normative anthropometric data derived from MRI in pediatric orbital anatomy remain limited. Thus, the present study aims to establish normative anthropometric reference values of critical orbital parameters in a pediatric cohort using MRI. Furthermore, the study assesses age-related variations and determines interobserver reliability among expert neuroradiologists to ensure methodological precision and reproducibility.

Methods

Study Population

This retrospective study included 64 healthy pediatric patients (32 males and 32 females) aged between 1 and 17 years (mean 10.37 ± 4.72 years). Patients were stratified into three distinct developmental groups: preschool (1–6 years), school-age (7–12 years), and adolescent (13–17 years). Inclusion criteria consisted of MRI examinations performed for non-orbital indications, with no known orbital or craniofacial abnormalities, trauma, or neurological conditions. Due to the retrospective nature of the study, the sample size was based on all available MRI scans meeting inclusion criteria within the defined study period, rather than on a formal statistical power analysis. Ethical approval was obtained from the institutional review board, and informed consent was waived due to the retrospective study design.

Imaging Protocol

MRI scans were acquired using either a 1.5 Tesla MRI scanner (Siemens, Erlangen, Germany; n = 28) or a 3 Tesla MRI scanner (Philips Healthcare, Best, Netherlands; n = 36). For both scanners, imaging included a single high-resolution isotropic 3D T2-weighted turbo spin echo (TSE) sequence (TR: 3500–4000 ms, TE: 90–100 ms, slice thickness: 1 mm, interslice gap: 0 mm, matrix size: 512×512, field of view: 180–220 mm), as well as a high-resolution isotropic 3D T1-weighted sequence acquired with comparable spatial resolution parameters. Due to the high-resolution protocol and small voxel sizes, an adequate signal-to-noise ratio (SNR) was ensured by using dedicated pediatric head coils designed for improved sensitivity and signal reception. Techniques such as increasing the number of signal averages (NSA = 2–3, depending on patient size) and employing partial Fourier encoding were utilized to optimize SNR without substantially prolonging scan time or compromising patient comfort. The isotropic datasets acquired from both T1 and T2 sequences were reconstructed into axial, coronal, and sagittal planes, and both sequence types were utilized for detailed orbital anthropometric measurements to optimize anatomical landmark visualization.

Orbital Anthropometric Measurements

Three experienced neuroradiologists independently performed all MRI measurements, with each neuroradiologist blinded to the others' results. All anthropometric measurements were systematically recorded using dedicated imaging analysis software (RadiAnt DICOM Viewer, Medixant, Poznan, Poland).

Extraocular muscle thicknesses, including the superior, inferior, medial, and lateral rectus muscles, were measured in axial, sagittal, and coronal planes. For each muscle, the measurement was consistently taken at the maximal cross-sectional diameter (the mid-belly region) and perpendicular to the muscle's long axis, explicitly accounting for their oblique anatomical orientations. To minimize variability associated with gaze position, only MRI scans acquired with the eyes in neutral (straightforward) gaze were selected for analysis (Fig. 1).

Orbital breadth and height were measured using coronal MRI images selected precisely at the mid-orbit plane, defined anatomically as the slice passing through the center of the optic nerve and the globe's maximal transverse diameter. Orbital breadth was recorded horizontally between the medial and lateral orbital walls at their maximal transverse dimension. Orbital height was measured vertically at the same coronal plane, spanning from the superior orbital roof directly downward to the lowest midpoint of the inferior orbital floor, explicitly considering the slope of the orbital floor. Measurements were taken perpendicular to the long axis of the orbit to ensure consistency and reproducibility (Fig. 2).

Interzygomatic distance was defined as the maximal transverse distance between the anterior margins of the bilateral zygomatic bones, clearly visualized on axial MRI images. Intercanthal distance was measured as the linear distance between bilateral medial canthi. The distance from the interzygomatic reference line, defined as the line connecting the anterior margins of the bilateral zygomatic bones, to the posterior margin of the globe was measured bilaterally, providing a consistent anterior-posterior reference of the globe's position within the orbit (Fig. 2).

Optic nerve sheath width was measured bilaterally at the midpoint of the intraorbital optic nerve segment rather than immediately posterior to the globe. Measuring at the midpoint was chosen deliberately to minimize variability resulting from localized expansions or anatomical variations occurring close to the globe, thus ensuring reproducible and clinically relevant normative values (Fig. 2).

The optic nerve angle was measured bilaterally on axial MRI images, specifically defined as the angle formed between the canalicular segment of the optic nerve (as it traverses the optic canal) and the midline sagittal plane. This measurement quantifies the divergence of the optic nerve from the mid-sagittal axis within the optic canal, providing clinically meaningful normative data for use in surgical planning and evaluation of pathologies involving the orbital apex or optic canal region (Fig. 2).

Statistical Analysis

Statistical analyses were conducted using SPSS software version 26.0 (IBM Corp., Armonk, NY, USA). Data were presented as mean ± standard deviation, median, and interquartile range (IQR). Spearman's correlation coefficient was used to assess correlations between orbital parameters and age. Group comparisons were made using Kruskal–Wallis tests followed by post-hoc Mann–Whitney U tests. Interobserver reliability was evaluated using intraclass correlation coefficients (ICC) with a two-way random-effects model assessing absolute agreement. Statistical significance was defined as $p < 0.05$.

Results

This MRI-based study included 64 pediatric patients (32 males, 32 females) aged 1–17 years (mean 10.37 ± 4.72 years) (Table 1). No significant difference in age distribution was observed between genders (p=0.8), allowing collective analysis for all orbital anthropometric measurements (Table 2).

Table 1. Demographic and clinical characteristics of the study population. Data are presented as numbers (n), mean ± standard deviation (SD), or median with interquartile range (IQR). BMI: Body Mass Index. All patients were free of known systemic or craniofacial diseases and underwent MRI examinations for non-orbital indications.

Characteristic	Value
Number of patients	64
Gender (Male/Female)	32 / 32
Age (years)	
Minimum	1
Maximum	17
Mean ± SD	10.37 ± 4.72
Median (IQR)	11 (7.25–14)
Age Group Distribution	
Pre-school (1–6 years)	13
School-age (7–12 years)	23
Adolescent (13–17 years)	28
Race/Ethnicity	All participants Caucasian
BMI (kg/m²)	17.2 ± 2.4 (normal range)
Systemic diseases (Diabetes, etc.)	None

Table 2. Age distribution of the study population according to gender. Data are presented as minimum (Min), maximum (Max), mean, standard deviation (Std Dev), median, and interquartile range (IQR). The p-

value was obtained using an independent samples t-test, indicating no statistically significant difference between male and female participants regarding age.

Participants	Age						
	Min	Max	Mean	Std Dev	Median	IQR	p-value
Male (n=32)	1	17	10.234	5.0032	10	7.25-15	0.8
Female (n=32)	1	17	10.516	4.4964	11.5	7.25-14	
All (n=64)	1	17	10.37	4.72	11	7.25-14	-

Detailed MRI measurements of extraocular muscle thicknesses, orbital breadth, orbital height, interzygomatic line length, intercanthal distance, distance from the interzygomatic line to the posterior margin of the globe, optic nerve sheath width, and optic nerve angle are summarized in Table 3. Notably, significant positive correlations were identified between age and several orbital parameters. The strongest correlation was observed with interzygomatic line length (Spearman's $r=0.772$, $p<0.001$).

Table 3. Demographic data and orbital anthropometric measurements across different pediatric age groups. Parameters are expressed as median with interquartile range (IQR). Correlation coefficients (r-values) represent the Spearman correlation between age and each orbital measurement. Statistical significance among age groups was tested using the Kruskal-Wallis test, and corresponding p-values are provided. Measurements are given in millimeters (mm) unless otherwise specified. M/F: Male/Female; SRM: Superior Rectus Muscle; IRM: Inferior Rectus Muscle; MRM: Medial Rectus Muscle; LRM: Lateral Rectus Muscle.

Parameter	Pre-school Median (IQR)	School-age Median (IQR)	Adolescent Median (IQR)	Correlation (r)	p-value
Age (years, Mean±SD)	4.5 (3.5-5)	10.0 (8-11)	15.0 (14-16)	-	-
Gender (M/F)	6/7	11/12	15/13	-	-
SRM (Sagittal) (mm)					
Right	2.4 (2.0-2.7)	2.3 (1.9-2.6)	2.5 (2.4-2.9)	0.610	**0.001**
Left	2.2 (1.9-2.6)	2.2 (1.9-2.5)	2.5 (2.1-2.8)	0.561	**0.001**
SRM (Coronal) (mm)					
Right	2.4 (2.2-2.8)	2.5 (2.2-2.7)	2.7 (2.3-3.1)	0.464	**0.006**
Left	2.5 (2.2-2.8)	2.4 (2.3-2.7)	2.6 (2.2-3.2)	0.450	**0.012**
IRM (Sagittal) (mm)					
Right	2.2 (1.8-2.5)	2.0 (1.0-2.5)	2.4 (2.2-2.6)	0.467	**0.001**
Left	2.1 (1.9-2.4)	2.1 (1.8-2.3)	2.3 (2.0-2.5)	0.484	**0.001**
IRM (Coronal) (mm)					
Right	2.4 (2.2-2.7)	2.4 (2.2-2.6)	2.6 (2.4-2.9)	0.495	**0.001**
Left	2.5 (2.1-2.8)	2.5 (2.0-2.8)	2.7 (2.4-2.8)	0.413	**0.01**
MRM (Axial) (mm)					
Right	2.5 (2.1-2.8)	2.4 (2.0-2.8)	2.7 (2.5-3.0)	0.680	**0.001**
Left	2.5 (2.1-2.8)	2.4 (2.0-2.8)	2.8 (2.4-3.1)	0.602	**0.001**
LRM (Axial) (mm)					
Right	2.1 (2.0-2.6)	2.1 (1.7-2.6)	2.4 (2.1-2.6)	0.440	**0.002**
Left	2.2 (2.0-2.6)	2.2 (1.8-2.5)	2.5 (2.1-2.8)	0.478	**0.002**
Orbital Breadth (mm)					
Right	33.6 (31.6-34.9)	32.5 (31.3-34.1)	34.8 (34.1-35.6)	0.674	**0.001**
Left	33.6 (31.9-35.3)	32.9 (31.6-34.0)	35.5 (33.9-36.9)	0.703	**0.001**
Orbital Height (mm)					
Right	38.8 (37.3-39.9)	38.6 (37.3-39.9)	39.5 (38.9-40.6)	0.608	**0.001**

Left	38.6 (36.9-40.0)	38.1 (36.7-39.2)	39.8 (38.7-41.7)	0.644	**0.001**
Interzygomatic Line (mm)	91.5 (85.5-97.0)	90.0 (85.1-92.8)	95.1 (92.9-97.8)	0.772	**0.001**
Interchantal Distance (mm)	21.9 (20.8-24.0)	21.8 (20.9-24.0)	23.6 (21.7-24.9)	0.517	**0.001**
Interzygomatic Line-Posterior Margin of Globe (mm)					
Right	7.3 (6.2-9.2)	7.2 (6.2-10.0)	6.8 (5.5-9.7)	0.38	0.08
Left	7.3 (6.3-9.4)	7.3 (6.7-10.0)	7.1 (5.7-8.2)	0.36	0.27
Optic Nerve Sheath Width (mm)					
Right	2.6 (2.3-3.1)	2.5 (2.3-3.2)	2.8 (2.5-3.0)	0.29	0.64
Left	2.6 (2.4-3.1)	2.6 (2.2-3.1)	2.8 (2.5-3.1)	0.27	0.33
Optic Nerve Angle (Degrees)					
Right	35.3 (32.7-37.1)	34.5 (33.3-37.0)	36.2 (32.8-37.9)	0.25	0.22
Left	35.3 (33.2-36.9)	35.4 (34.1-36.8)	35.7 (33.1-38.0)	0.20	0.31

Orbital breadth and height also demonstrated strong, significant correlations with age (orbital breadth right: r=0.674; left: r=0.703; orbital height right: r=0.608; left: r=0.644; all p<0.001).

Interobserver reliability, assessed via intraclass correlation coefficients (ICC), demonstrated excellent consistency among measurements performed independently by three neuroradiologists (Table 4). Orbital breadth (ICC=0.92, 95% CI: 0.89–0.95) and orbital height (ICC=0.90, 95% CI: 0.87–0.93) showed the highest reliability, underscoring the robustness of the MRI-based measurement methodology.

Table 4. Intraclass correlation coefficient (ICC) values demonstrating interobserver reliability for orbital anthropometric measurements. Measurements were independently performed by three neuroradiologists. ICC values include 95% confidence intervals (CI), with interpretation provided based on standard reliability guidelines (Excellent: ICC>0.90, Good: ICC 0.75–0.90). SRM: Superior Rectus Muscle; IRM: Inferior Rectus Muscle; MRM: Medial Rectus Muscle; LRM: Lateral Rectus Muscle.

Parameter	ICC (95% CI)	Interpretation
SRM (Sagittal) (mm)		
Right	0.93 (0.90–0.96)	Excellent reliability
Left	0.92 (0.89–0.95)	Excellent reliability
SRM (Coronal) (mm)		
Right	0.91 (0.88–0.94)	Excellent reliability
Left	0.91 (0.88–0.94)	Excellent reliability
IRM (Sagittal) (mm)		
Right	0.90 (0.87–0.93)	Excellent reliability
Left	0.89 (0.86–0.92)	Good reliability
IRM (Coronal) (mm)		
Right	0.91 (0.88–0.94)	Excellent reliability
Left	0.90 (0.87–0.93)	Excellent reliability
MRM (Axial) (mm)		
Right	0.92 (0.89–0.95)	Excellent reliability
Left	0.91 (0.88–0.94)	Excellent reliability
LRM (Axial) (mm)		
Right	0.88 (0.84–0.91)	Good reliability
Left	0.87 (0.83–0.90)	Good reliability
Orbital Breadth (mm)		
Right	0.92 (0.89–0.95)	Excellent reliability
Left	0.91 (0.88–0.94)	Excellent reliability
Orbital Height (mm)		
Right	0.90 (0.87–0.93)	Excellent reliability
Left	0.90 (0.87–0.93)	Excellent reliability
Interzygomatic Line (mm)	0.88 (0.84–0.91)	Good reliability
Interchantal Distance (mm)	0.85 (0.80–0.89)	Good reliability
Interzygomatic Line-Posterior Margin of Globe (mm)		
Right	0.87 (0.83–0.91)	Good reliability

Left	0.86 (0.82–0.90)	Good reliability
Optic Nerve Sheath Width (mm)		
Right	0.88 (0.84–0.91)	Good reliability
Left	0.87 (0.83–0.90)	Good reliability
Optic Nerve Angle (Degrees)		
Right	0.85 (0.80–0.89)	Good reliability
Left	0.84 (0.79–0.88)	Good reliability

Discussion

This study provides comprehensive MRI-based normative data on orbital anthropometric parameters in a healthy pediatric population, highlighting MRI as a radiation-free imaging technique suitable for detailed assessment of orbital anatomy. Our findings clearly highlight age-related variations in several orbital dimensions, including orbital breadth, orbital height, interzygomatic line length, intercanthal distance, optic nerve sheath width, optic nerve angle, and thickness of the extraocular muscles. These measurements are aligned with existing literature derived from various imaging modalities and populations, thereby reinforcing the robustness and clinical utility of our results.

The significant positive correlation observed between age and orbital parameters, particularly notable in the interzygomatic line length (Spearman's $r = 0.772$, $p < 0.001$), confirms previous findings reported by Escaravage and Dutton, who demonstrated similar growth trajectories using CT imaging [10]. Previously, Gupta et al. provided normative data on orbital measurements derived from computed tomography in an adult population, emphasizing the importance of establishing precise reference values for anatomical structures. Although their study was conducted primarily on adults with a mean age in the 30s and did not specifically investigate pediatric growth trends, their work reinforces the broader need for accurate and age-specific normative data across different demographic groups [11].

Orbital breadth and height measurements similarly demonstrated significant correlations with advancing age. A previous CT-based study by Pool et al. also reported comparable growth patterns, underlining consistent anatomical changes across diverse pediatric cohorts [12]. Furthermore, Kaplanoglu et al. emphasized comparable age-related trends in orbital measurements among adult populations, suggesting a continuity of growth patterns extending beyond adolescence [13].

Our rationale for categorizing the pediatric population into three broad age groups (pre-school, school-age, and adolescent) was guided by clinical and developmental considerations. These categories allowed clear differentiation of developmental phases, recognizing critical periods of rapid craniofacial growth. In contrast, studies like Almus et al. utilized narrower age groupings defined by months, offering insights into more nuanced developmental trajectories [14]. While our broader categorization provides

robust and clinically useful benchmarks, more granular divisions might offer additional detail, potentially beneficial for targeted clinical assessments and interventions.

The optic nerve sheath width and optic nerve angle measurements obtained in our study provided reliable and clear MRI-based normative data. Tsukitome et al. highlighted the relative anatomical stability of optic nerve angles in Japanese children, which aligns with our observations of minimal variations in optic nerve angles across age groups [15]. Conversely, a study by Maresky et al. documented significant variability in optic nerve sheath diameters across pediatric populations, emphasizing the necessity for precise normative reference data, such as those generated by our study, for improved clinical diagnostics and management [16].

Our detailed assessment of interobserver reliability revealed excellent reproducibility, notably high ICC values for orbital breadth (ICC = 0.92) and orbital height (ICC = 0.90). Previous studies have similarly underscored the high reliability of orbital anthropometric measurements across multiple imaging modalities, thereby bolstering the validity and applicability of our MRI-based measurement protocol. This consistency further enhances clinical confidence in the robustness of MRI for pediatric orbital assessment [14, 17].

Additionally, our findings on intercanthal distance align closely with those reported by Pool et al., who emphasized the diagnostic significance of accurate interorbital and intercanthal measurements for early identification of craniofacial anomalies. Such parameters are crucial in surgical planning, especially in pediatric ophthalmology and craniofacial reconstructive interventions [12].

Bekerman et al. provided normative data regarding eyeball diameter in adults. Although our study did not specifically measure eyeball diameter and focused exclusively on pediatric orbital anthropometric parameters, Bekerman et al.'s study underscores the general importance of establishing precise normative anatomical reference data in ophthalmologic and radiological contexts [18]. However, given the clear differences in anatomical measurements and the demographic groups studied, direct validation or comparison between their findings and our pediatric orbital data is not possible. Future investigations that directly correlate pediatric orbital measurements with ocular parameters across age groups could further enhance clinical utility.

Further enriching the comparative context, Wei et al. documented detailed orbital volume measurements across a wide pediatric age range, reinforcing our findings of significant orbital dimensional changes corresponding to developmental stages [19]. Similarly, other studies introduced normative orbital indices that underscore racial and gender-specific variability, highlighting the importance of establishing diverse normative datasets to enhance diagnostic precision [20–23].

Clinically, the normative MRI-based orbital anthropometric data provided by our study have substantial implications. Accurate reference values facilitate early detection and improved management of orbital pathologies, including traumatic injuries, congenital anomalies, thyroid-associated orbitopathy, and

orbital tumors. Precise anthropometric reference data are crucial for optimizing surgical outcomes and enhancing clinical management strategies.

Several limitations must be acknowledged. Our retrospective study design and relatively limited sample size potentially restrict generalizability. A significant methodological limitation relates to the inherent challenges of MRI in precisely identifying certain bony landmarks compared to computed tomography (CT). Specifically, delineating precise anatomical reference points on MRI, such as the orbital roof, orbital floor, and medial and lateral orbital walls, can be more difficult due to MRI's superior soft-tissue contrast but inferior bone-to-soft tissue differentiation compared to CT. Additionally, certain measurement landmarks, including the anterior margin of the zygomatic bone, may appear less distinctly defined on MRI, potentially increasing interobserver variability and measurement uncertainty.

Another important limitation concerns imaging resolution, specifically the 1-mm slice thickness utilized in our MRI protocols. Although considered high-resolution for routine clinical MRI, this slice thickness inherently limits measurement precision due to partial-volume effects, particularly for smaller anatomical structures that approach voxel dimensions. Such resolution limitations may contribute to measurement discrepancies and reduced accuracy in the assessment of subtle anatomical features.

Moreover, orbital measurements performed on axial MRI images exhibited slightly greater interobserver variability compared to measurements in other imaging planes, likely due to the anatomical complexity and obliquity of orbital structures as visualized in axial sections. The inherent oblique orientation of structures such as the extraocular muscles, optic nerve, and orbital walls increases ambiguity when defining landmarks in axial views, thus affecting observer consistency. These methodological challenges were partly mitigated by employing standardized imaging protocols, clearly defined anatomical landmarks, and consistent measurement practices.

Future studies directly comparing MRI and CT measurements or employing isotropic high-resolution 3D MRI sequences with smaller voxel sizes could further clarify these methodological nuances, enhance measurement precision, and validate the clinical applicability of MRI-based normative anthropometric data.

Conclusions

Our study demonstrates that MRI provides a reliable, radiation-free modality for detailed anthropometric assessment of pediatric orbital anatomy, generating comprehensive normative data that can serve as essential reference points in clinical practice. These MRI-based normative measurements may enhance the accuracy of diagnosing orbital abnormalities, assist clinicians and surgeons in identifying developmental anomalies, and provide valuable benchmarks for surgical planning in pediatric populations.

Declarations

Disclosure

The authors declare no conflicts of interest relevant to this manuscript.

Author Contribution

C.I.G. and A.A. designed the study, analyzed and interpreted the data, and wrote the manuscript.E.H.K., E.K., Z.B., M.S.C., G.D., S.S., and M.B. collected the data, performed measurements, and participated in manuscript preparation.All authors critically reviewed, revised, and approved the final manuscript.

Acknowledgment

The authors gratefully acknowledge the contributions of the radiology staff and neuroradiologists who assisted in obtaining and interpreting the MRI scans utilized in this study. Their dedicated effort and expertise were essential for the successful completion of this research.

References

1. Betts AM, O'Brien WT, Davies BW, Youssef OH (2014) A systematic approach to CT evaluation of orbital trauma. Emerg Radiol 21:511–531. https://doi.org/10.1007/S10140-014-1221-5
2. Ferreira TA, Saraiva P, Genders SW et al (2018) CT and MR imaging of orbital inflammation. Neuroradiology 60:1253–1266. https://doi.org/10.1007/S00234-018-2103-4
3. Weaver AA, Loftis KL, Tan JC et al (2010) CT based three-dimensional measurement of orbit and eye Anthropometry. Invest Ophthalmol Vis Sci 51:4892–4897. https://doi.org/10.1167/IOVS.10-5503
4. Kolk A, Pautke C, Schott V et al (2007) Secondary Post-Traumatic Enophthalmos: High-Resolution Magnetic Resonance Imaging Compared With Multislice Computed Tomography in Postoperative Orbital Volume Measurement. J Oral Maxillofac Surg 65:1926–1934. https://doi.org/10.1016/j.joms.2006.06.269
5. Furuta M (2001) Measurement of orbital volume by computed tomography: Especially on the growth of the orbit. Jpn J Ophthalmol 45:600–606. https://doi.org/10.1016/S0021-5155(01)00419-1
6. Mathews JD, Forsythe AV, Brady Z et al (2013) Cancer risk in 680 000 people exposed to computed tomography scans in childhood or adolescence: Data linkage study of 11 million Australians. BMJ (Online) 346. https://doi.org/10.1136/BMJ.F2360
7. Pearce MS, Salotti JA, Little MP et al (2012) Radiation exposure from CT scans in childhood and subsequent risk of leukaemia and brain tumours: A retrospective cohort study. Lancet 380:499–505. https://doi.org/10.1016/S0140-6736(12)60815-0
8. Brenner DJ, Hall EJ (2007) Computed Tomography — An Increasing Source of Radiation Exposure. N Engl J Med 357:2277–2284. https://doi.org/10.1056/NEJMRA072149

9. Ettl A, Kramer J, Daxer A, Koornneef L (1997) High-resolution magnetic resonance imaging of the normal extraocular musculature. Eye 11:793–797. https://doi.org/10.1038/EYE.1997.207
10. Escaravage GK, Dutton JJ (2013) Age-related changes in the pediatric human orbit on CT. Ophthalmic Plast Reconstr Surg 29:150–156. https://doi.org/10.1097/IOP.0B013E3182859716
11. Gupta V, Prabhakar A, Yadav M, Khandelwal N (2019) Computed tomography imaging-based normative orbital measurement in Indian population. Indian J Ophthalmol 67:659–663. https://doi.org/10.4103/IJO.IJO_1187_18
12. Pool GM, Didier RA, Bardo D et al (2016) Computed tomography-generated anthropometric measurements of orbital relationships in normal infants and children. J Neurosurg Pediatr 18:201–206. https://doi.org/10.3171/2016.2.PEDS15475
13. Kaplanoglu V, Kaplanoglu H, Toprak U et al (2014) Anthropometric Measurements of the orbita and gender prediction with three-dimensional computed tomography images. Folia Morphologica (Poland) 73:149–152. https://doi.org/10.5603/FM.2014.0022
14. Almus E, Sen Akova B, Ozer H, Fitoz S (2022) Orbital structures in the pediatric age group: A normative assessment using magnetic resonance imaging. Eur J Radiol 154. https://doi.org/10.1016/J.EJRAD.2022.110418
15. Tsukitome H, Hatsukawa Y, Morimitsu T et al (2015) Changes in angle of optic nerve and angle of ocular orbit with increasing age in Japanese children. Br J Ophthalmol 99:263–266. https://doi.org/10.1136/BJOPHTHALMOL-2014-305236
16. Maresky HS, Ben Ely A, Bartischovsky T et al (2018) MRI measurements of the normal pediatric optic nerve pathway. J Clin Neurosci 48:209–213. https://doi.org/10.1016/j.jocn.2017.11.015
17. Al-Haddad CE, Sebaaly MG, Tutunji RN et al (2018) Optic Nerve Measurement on MRI in the Pediatric Population: Normative Values and Correlations. Am J Neuroradiol 39:369–374. https://doi.org/10.3174/AJNR.A5456
18. Bekerman I, Gottlieb P, Vaiman M (2014) Variations in Eyeball Diameters of the Healthy Adults. J Ophthalmol. https://doi.org/10.1155/2014/503645
19. Wei N, Bi H, Zhang B et al (2017) Biphasic growth of orbital volume in Chinese children. Br J Ophthalmol 101:1162–1167. https://doi.org/10.1136/BJOPHTHALMOL-2016-309848
20. Lee JS, Lim DW, Lee SH et al (2001) Normative measurements of Korean orbital structures revealed by computerized tomography. Acta Ophthalmol Scand 79:197–200. https://doi.org/10.1034/J.1600-0420.2001.079002197.X
21. Burns NS, Iyer RS, Robinson AJ, Chapman T (2013) Diagnostic imaging of fetal and pediatric orbital abnormalities. Am J Roentgenol 201. https://doi.org/10.2214/AJR.13.10949
22. Ozgen A, Ariyurek M (1998) Normative measurements of orbital structures using CT. Am J Roentgenol 170:1093–1096. https://doi.org/10.2214/AJR.170.4.9530066
23. Wi JM, Sung KH, Chi M (2017) Orbital volume restoration rate after orbital fracture; A CT-based orbital volume measurement for evaluation of orbital wall reconstructive effect. Eye (Basingstoke) 31:713–719. https://doi.org/10.1038/EYE.2016.311

Figures

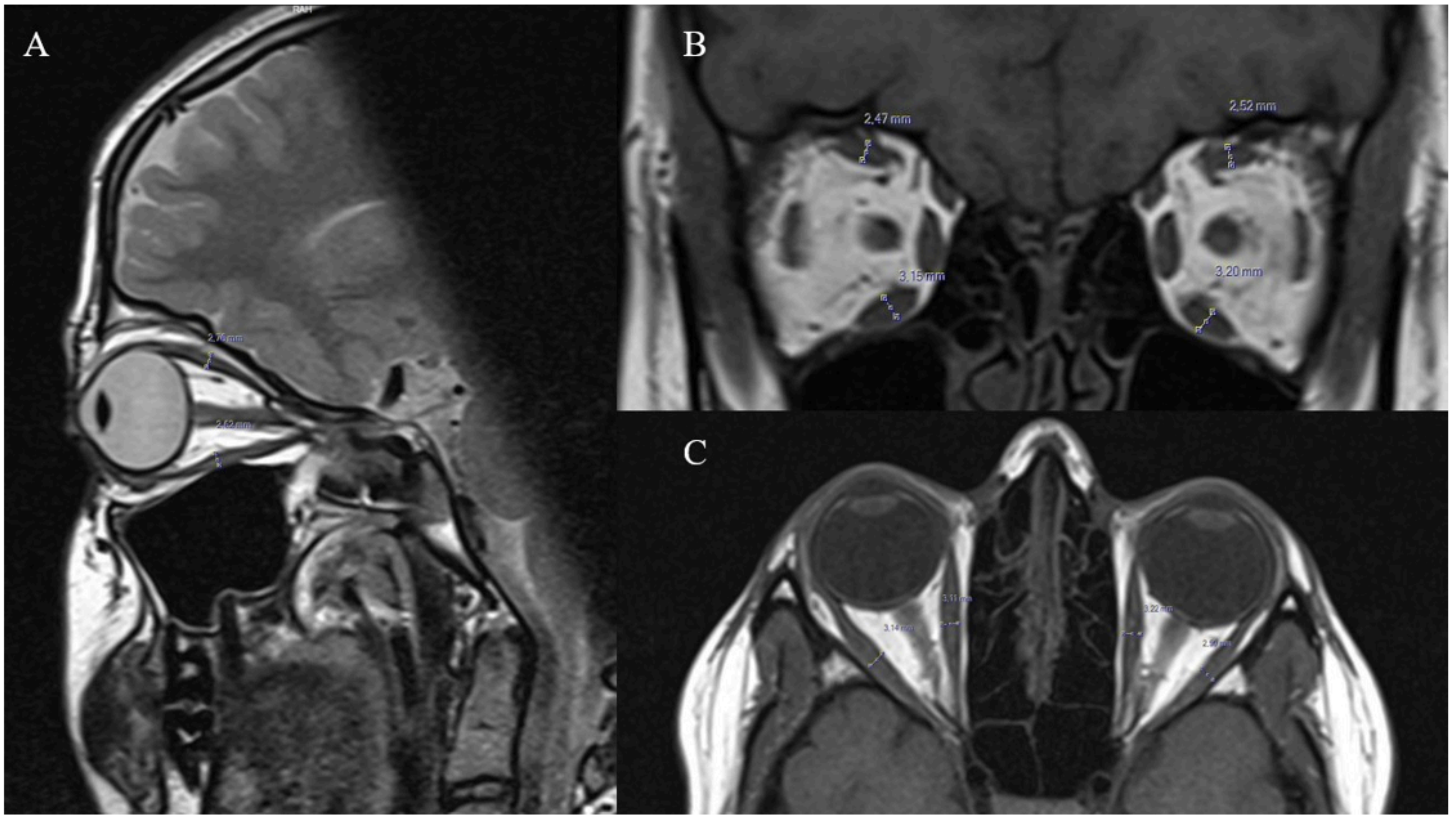


Figure 1

MRI images illustrating the standardized approach for measuring extraocular muscle thicknesses in pediatric orbital anthropometry. Measurements were consistently performed at the maximal cross-sectional diameter ("mid-belly" region) of each muscle, perpendicular to the muscle's long axis, explicitly accounting for their oblique anatomical orientation. To ensure consistency and minimize variability due to gaze direction, only images with eyes in a neutral (straightforward) gaze position were used. **(A)** Sagittal plane demonstrating measurement sites for the superior rectus muscle (SRM) and the inferior rectus muscle (IRM). **(B)** Coronal plane illustrating measurement points for the superior rectus muscle (SRM) and the inferior rectus muscle (IRM). **(C)** Axial plane depicting measurement technique for medial rectus muscle (MRM) and lateral rectus muscle (LRM), clearly showing oblique measurement orientation aligned perpendicularly to muscle axes.

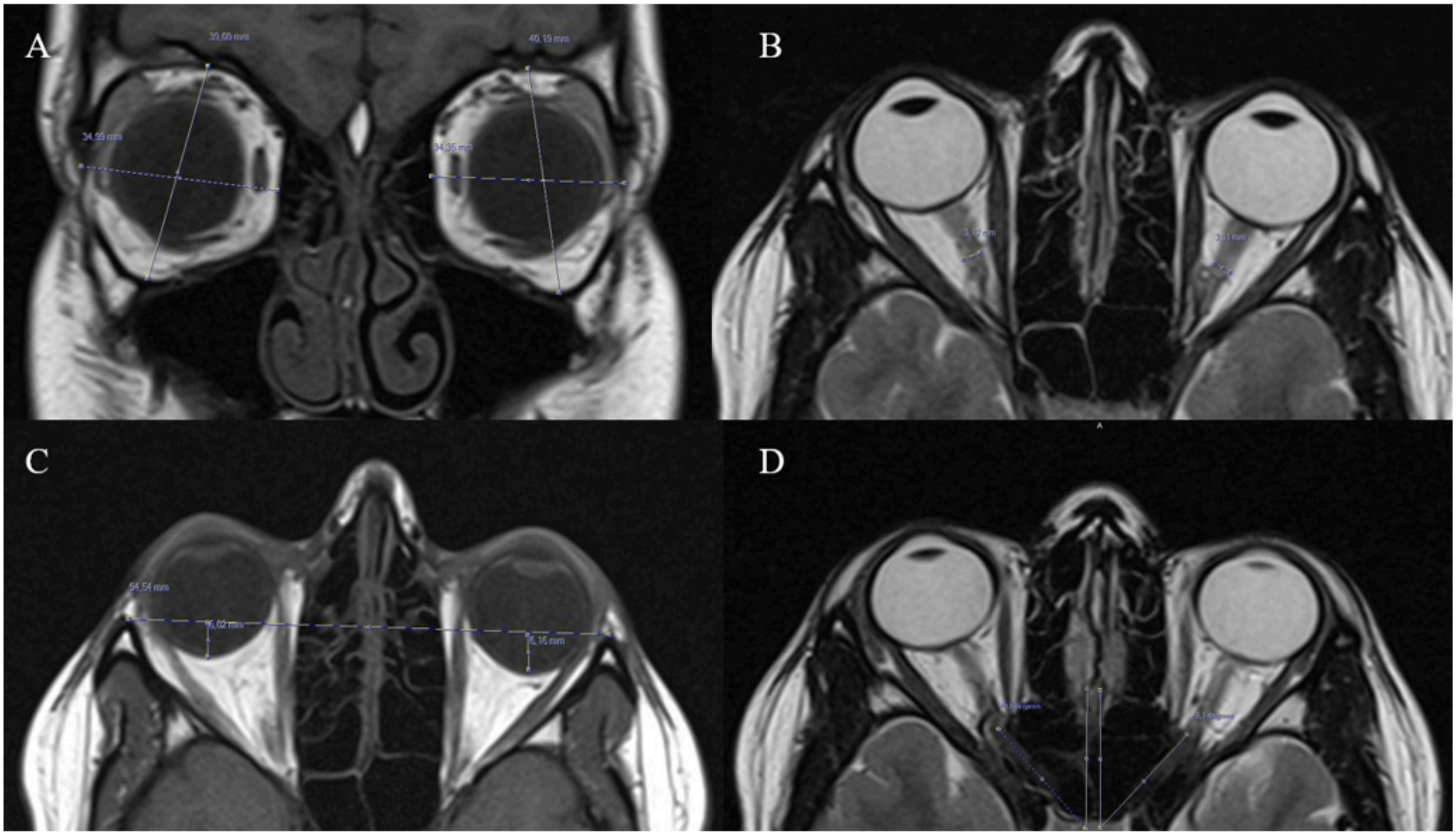


Figure 2

MRI images illustrating key orbital anthropometric measurements utilized in the study. (A) Coronal T1-weighted image demonstrating measurements of orbital breadth and orbital height. (B) Axial T2-weighted image depicting measurements of the optic nerve sheath width at the mid-intraorbital segment. (C) Axial T1-weighted image showing measurements of interzygomatic line length between anterior margins of the bilateral zygomatic bones, and the distance from the interzygomatic line to the posterior margin of the globe. (D) Axial T2-weighted image illustrating measurement of the optic nerve angle bilaterally, defined as the angle between the canalicular segment of the optic nerve and the midline sagittal plane. All anthropometric measurements were confirmed and cross-validated using both T1- and T2-weighted images to ensure optimal accuracy and consistency.